ACS OMEGA

Open Access

http://pubs.acs.org/journal/acsodf

Article

Green One-Pot Synthesis of Thiazole Scaffolds Catalyzed by Reusable $NiFe_2O_4$ Nanoparticles: *In Silico* Binding Affinity and *In Vitro* Anticancer Activity Studies

Satish Gudala,* Archi Sharma,* Aruna Lankada, Ruotong Liu, Anubhuti Jha, Santhosh Penta,* Owias Iqbal Dar, and Jianxin Yang*

Cite This: *ACS Omega* 2024, 9, 38262−38271

Read Online

ACCESS | Metrics & More | Article Recommendations | Supporting Information

ABSTRACT: A facile, green, one-pot multicomponent synthesis strategy was employed to fabricate novel thiazole scaffolds incorporating phthalazine, pyridazine, and pyrido-pyridazine derivatives (**4a**−**4o**). This synthetic route entailed the reaction of an α-halo carbonyl compound (**1**) with thiosemicarbazide (**2**) and various anhydrides (**3a**−**3o**), utilizing $NiFe_2O_4$ nanoparticles as a reusable catalyst in an ethanol:water (1:1) solvent system. The cytotoxicity of the synthesized compounds was meticulously assessed against three cancer cell lines, A375, HeLa, and MCF-7, employing IC_{50} values (μM) as the benchmark, and compared to the reference drug erlotinib. Compound **4n** displayed remarkable efficacy against A375 (0.87 ± 0.31 μM), HeLa (1.38 ± 1.24 μM), and MCF-7 (1.13 ± 0.96 μM) cell lines, significantly surpassing erlotinib's IC_{50} values. Additionally, compounds **4k**, **4l**, **4m**, and **4o** demonstrated notable cytotoxicity across all tested cell lines, indicating their potential as effective anticancer agents. *In silico* docking studies against Hsp82 and Hsp90 proteins indicated that ligands **4k**, **4m**, **4c**, **4j**, **4o**, and **4l** had superior binding affinities compared to erlotinib. ADME analysis showed that compounds **4n**, **4j**, **4l**, **4m**, and **4o** had favorable pharmacokinetic profiles, including nontoxicity, high human intestinal absorption, and low CYP inhibitory promiscuity. Structure−activity relationship analysis revealed that cyano and benzylidene substitutions significantly enhanced anticancer activity. Overall, the synthesized compounds, particularly **4n**, demonstrated high efficacy, favorable binding interactions, and promising pharmacokinetic profiles, making them strong candidates for further development as anticancer agents.

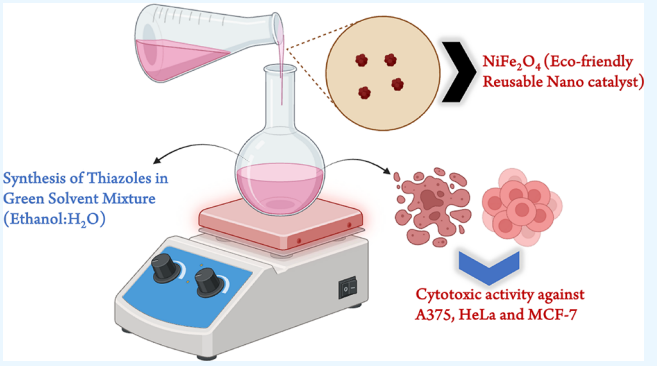

INTRODUCTION

Cancer is one of the main reasons for almost 13% of all deaths worldwide in spite of substantial work being done toward the progress of efficient anticancer therapies. In the next two decades, the number of new cases is predicted to rise by about 70%.[1] The International Agency for Research on Cancer (IARC) of the World Health Organization released the most recent global cancer data in 2020. The data showed that there were 19.29 million new cases of cancer worldwide in 2020 (10.06 million males and 9.23 million females), with 4.57 million (23.7%) of those cases occurring in China. Also, 9.96 million cancer deaths occurred worldwide, with 3 million of those deaths occurring in China. This is nearly 30% of all cancer deaths with the highest cancer rate worldwide.[2,3] The development of novel, efficient, and effective antiproliferative agents among small molecules has proven to be a productive and dynamic tactic in managing and treating cancer, despite the advancements in cancer control and prevention approaches, early diagnostics techniques, and the use of personalized chimeric antigen receptor (CAR) T-cell therapy and immunotherapy with monoclonal antibodies.[4] Hence, the development of novel and potent anticancer drugs with promising activity may be possible through the design of drug-like molecules for the treatment of cancer. The primary focus of the structure-based drug design methodology has been the identification of potential molecular scaffolds or building blocks for the synthesis of pharmacologically active compounds. Furthermore, nitrogen-containing heterocycle compounds have been widely identified for their anticancer activities.[5]

Among them, thiazole is an important nitrogen-containing heterocycle that can be synthesized by some common routes like Hantzsch, Tchernic, Cook−Heliborn, and Gabriel methods.[6] Thiazoles have significant biological activities

Received: July 3, 2024
Revised: August 20, 2024
Accepted: August 23, 2024
Published: August 29, 2024

including antiviral,[7] antiparasitic,[8] antifungal,[9] antibacterial,[10] antioxidant,[11] and antiproliferative activities.[12] Similarly, sulfonamide[13] and pyrimidine derivatives[14] are being reported with diversified biological activities. Moreover, the recent literature reveals that thiazolo-pyrimidine derivatives showed many activities including anticancer activity against A375 (melanoma), HeLa (cervical cancer), and MCF-7 (breast carcinoma) cancer lines.[15−17] The most renowned anticancer drugs like dabrafenib[18,19] [i], dasatenib[20,21] [ii], and pazopanib[22−24] [iii] have either pyrimidines, thiazole, or sulfonamide linkage moieties (Figure 1) in their structures

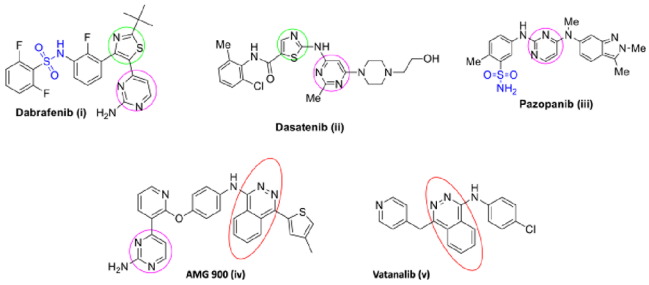

Figure 1. Structures of some bioactive scaffolds.

and proved good activities on these cell lines. On the other hand, several phthalazine derivatives also displayed a wide range of pharmacological properties including anticancer activities against these cell lines.[25,26] They were found as various enzymatic and specific cell proliferative targets. For instance, AMG 900 [iv] is a selective aurora kinase inhibitor[27] and vatanalib [v] is a tyrosine kinase inhibitor.[28] Thus, synthesis of integrated biomolecules comprising pyrimidinyl−phthalazinyl−thiazole scaffolds will be attractive from a synthetic as well as a pharmaceutical point of view.

Conversely, one-pot, multicomponent reaction (MCR) is one of the most convenient methods for the synthesis of bioactive compounds due to its higher selectivity, greater atom economy, shorter reaction time, and cost effectiveness.[29,30] Recently, nanoparticle-catalyzed MCRs have attracted considerable interest because of their higher surface areas, high selectivity, and reusability.[31] Moreover, magnetic NPs, namely, ferrite nanoparticles, provide an added advantage of easy separation by an external magnet from the reaction mixture.[32,33] In addition, the choice of the solvent in a chemical reaction also plays a crucial role in organic synthesis. In the context of green chemistry and over decades, remarkable efforts have been made for the development of synthetic methodologies in aqueous medium.[34,35]

As part of our continuous effort in green synthesis of biologically active scaffolds using nanoparticles as a reusable catalyst,[36] herein, we report one-pot, multicomponent synthesis of thiazole scaffolds using $NiFe_2O_4$ NPs as a reusable catalyst. The synthesized compounds were subjected to *in silico* docking studies targeting Hsp82 (*Saccharomyces cerevisiae*) and Hsp90 (*Homo sapiens*) receptors, *in vitro* anticancer activity against A375, HeLa, and MCF-7 cancer lines, and SAR evaluation. Additionally, ADME analysis was conducted to assess various pharmacokinetic parameters, elucidating the potential of the synthesized compounds as anticancer agents. An efficient method is delineated for the synthesis of novel thiazole scaffolds comprising phthalazine, pyridazine, and pyrido-pyridazine derivatives (**4a−4o**) through a $NiFe_2O_4$ nanoparticle-catalyzed one-pot, three-component reaction, as illustrated in Scheme 1. The synthesis involved the condensation of the α-halo carbonyl compound (**1**) with

Scheme 1. Synthesis of Thiazole Scaffolds Using $NiFe_2O_4$ NPs (4a−4o)

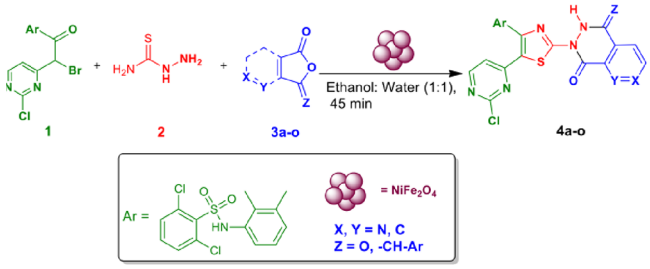

thiosemicarbazide (**2**) and various anhydrides in the presence of nano-$NiFe_2O_4$ and aqueous ethanol, facilitating the formation of desired products. The key intermediate α-bromo carbonyl compound (**1**) was prepared according to our reported procedure.[36]

EXPERIMENTAL SECTION

General Procedure. All the solvents and reagents were pure, purchased from available commercial sources, and were used without any additional purification. The final compounds were checked for purity by using TLC plates (E. Merck Mumbai, India). The analysis of CHNS was done by an automatic elemental analyzer, Carlo Erba EA 1108, Italy. IR spectra of all the synthesized compounds were recorded using KBr pellets on an FTIR spectrometer (PerkinElmer 100). ^{1}HNMR and ^{13}C NMR spectra were taken using TMS as standard (in δ ppm) on a Bruker Avance I spectrometer, Switzerland. A liquid chromatography quadrupole ion-trap mass spectrometer purchased from San Jose, California, USA (Thermo Finnigan), was used to determine the mass spectra (ESI-MS). Melting points were checked with a "Cintex" melting point apparatus in Mumbai, India, by using open capillaries and were uncorrected.

General Procedure for the Synthesis of Title Compounds 4a−4o. A mixture of *N*-(3-(2-bromo-2-(2-chloropyrimidin-4-yl)acetyl)-2-chlorophenyl)-2,6-dichlorobenzene sulfonamide (1 mmol), thiosemicarbazide (1 mmol), and various anhydrides (1 mmol) was combined with $NiFe_2O_4$ nanoparticles (5 mg) in 5 mL of an ethanol:water (1:1) solvent system. The resulting mixture was heated at 75 °C for 45−60 min, with the progress of the reaction monitored by TLC. After completion, the reaction mixture was cooled to room temperature and the solid product was filtered, washed with water, dried, and purified by recrystallization from absolute ethanol.

*2,6-Dichloro-N-(2-chloro-3-(5-(2-chloropyrimidin-4-yl)-2-(1,4-dioxo-3,4-dihydrophthalazin-2(1H)-yl)thiazol-4-yl)-phenyl)benzenesulfonamide (**4a**).* Pale-yellow solid, yield: 90% mp: 245−247 °C; ^{1}H NMR (δ ppm, DMSO-d_6, 300 MHz): 10.08 (s, 1H, amide, N−H), 8.67 (s, 1H, N−H), 8.21 (d, J = 9.0 Hz, 1H, CH, pyrimidine, Ar−H), 7.11−7.49 (m 8H, Ar−H), 6.88−6.94 (m, 2H, Ar−H), 6.61 (d, J = 9.0 Hz, 1H, CH, pyrimidine, Ar−H); ^{13}C NMR (δ ppm, DMSO-d_6, 75 MHz): 173.53, 167.64, 163.96, 160.51, 159.94, 159.67, 159.60, 156.53, 153.99, 150.66, 147.01, 135.53, 133.47, 131.78, 130.92, 129.44, 128.80, 128.52, 127.82, 127.53, 124.92, 124.22, 124.04, 122.97, 122.79, 117.10, 115.11.

https://doi.org/10.1021/acsomega.4c05587
ACS Omega 2024, 9, 38262−38271

*2,6-Dichloro-N-(2-chloro-3-(5-(2-chloropyrimidin-4-yl)-2-(5-methyl-1,4-dioxo-3,4-dihydrophthalazin-2(1H)-yl)thiazol-4-yl)phenyl)benzenesulfonamide (**4b**).* Yellow solid, yield: 88% mp: 251−253 °C; ^{1}H NMR (δ ppm, DMSO-d$_6$, 300 MHz): 10.09 (s, 1H, amide, N−H), 8.69 (s, 1H, N−H), 8.20−8.22 (d, J = 9.0 Hz, 1H, CH, pyrimidine, Ar−H), 7.08−7.49 (m 8H, Ar−H), 6.93−6.94(m, 2H, Ar−H), 6.62−6.64 (d, J = 9.0 Hz, 1H, CH pyrimidine, Ar−H), 2.46(S, 3H, CH$_3$); ^{13}C NMR (δ ppm, DMSO-d$_6$, 75 MHz): 173.34, 161.14, 160.32, 160.30, 160.23, 157.16, 154.63, 151.30, 147.65, 136.17, 131.56, 129.44, 129.15, 128.46, 128.17, 125.23, 124.85, 124.67, 123.55, 123.17, 116.65.

*2,6-Dichloro-N-(2-chloro-3-(2-(5-chloro-1,4-dioxo-3,4-dihydrophthalazin-2(1H)-yl)-5-(2-chloropyrimidin-4-yl)-thiazol-4-yl)phenyl)benzenesulfonamide (**4c**).* Yellow solid, yield: 86% mp: 256−258 °C; ^{1}H NMR (δ ppm, DMSO-d$_6$, 300 MHz): 10.09 (s, 1H, sulfonamide, N−H), 9.25 (s, 1H, N−H), 8.25−8.27 (d, J = 9.0 Hz, 1H, CH, pyrimidine, Ar−H), 7.00−7.70 (m 9H, Ar−H), 6.72−6.75 (d, J = 9.0 Hz, 1H, CH pyrimidine, Ar−H); ^{13}C NMR (δ ppm, DMSO-d$_6$, 75 MHz): 173.73, 161.35, 160.73, 160.09, 160.01, 159.94, 156.87, 154.33, 151.00, 147.35, 144.73, 141.09, 135.87, 134.12, 133.12, 132.74, 131.27, 129.14, 128.86, 128.16, 127.87, 126.86, 126.01, 125.26, 125.12, 124.74, 124.12, 123.87.

*2,6-Dichloro-N-(2-chloro-3-(2-(6-chloro-1,4-dioxo-3,4-dihydrophthalazin-2(1H)-yl)-5-(2-chloropyrimidin-4-yl)-thiazol-4-yl)phenyl)benzenesulfonamide (**4d**).* Pale-yellow solid, yield: 88% mp: 255−257 °C; ^{1}H NMR (δ ppm, DMSO-d$_6$, 300 MHz): 10.03 (s, 1H, sulfonamide, N−H), 8.76 (s, 1H, N−H), 8.16−8.19 (d, J = 9.0 Hz, 1H, CH, pyrimidine, Ar−H), 7.02−7.61 (m 8H, Ar−H), 6.63−6.66 (d, J = 9.0 Hz, 1H, CH pyrimidine, Ar−H); ^{13}C NMR (δ ppm, DMSO-d$_6$, 75 MHz): 173.70, 161.87, 160.86, 160.14, 160.01, 159.94, 156.87, 154.33, 151.00, 147.27, 144.14, 141.86, 135.87, 134.12, 133.12, 132.74, 131.27, 129.14, 128.86, 128.16, 127.87, 126.86, 126.14, 125.26, 125.17, 124.86, 124.01, 123.84.

*2,6-Dichloro-N-(2-chloro-3-(5-(2-chloropyrimidin-4-yl)-2-(6-methoxy-1,4-dioxo-3,4-dihydrophthalazin-2(1H)-yl)-thiazol-4-yl)phenyl)benzenesulfonamide (**4e**).* Pale-yellow solid, yield: 88% mp: 242−244 °C; ^{1}H NMR (δ ppm, DMSO-d$_6$, 300 MHz): 10.13 (s, 1H, sulfonamide, N−H), 8.28 (s, 1H, N−H), 8.16−8.19 (d, J = 9.0 Hz, 1H, CH, pyrimidine, Ar−H), 6.91−7.49 (m 8H, Ar−H), 6.63−6.66 (d, J = 9.0 Hz, 1H, CH pyrimidine, Ar−H), 3.74 (S, 3H, OCH$_3$); ^{13}C NMR (δ ppm, DMSO-d$_6$, 75 MHz): 173.61, 165.99, 161.41, 160.86, 160.00, 159.75, 159.68, 156.61, 154.07, 151.45, 150.74, 147.09, 135.61, 133.61, 131.07, 130.21, 128.88, 128.60, 127.90, 127.61, 126.55, 125.00, 124.30, 124.61, 123.07, 122.87, 117.15, 57.90.

*N-(3-(2-(5-Amino-1,4-dioxo-3,4-dihydrophthalazin-2(1H)-yl)-5-(2-chloropyrimidin-4-yl)thiazol-4-yl)-2-chlorophenyl)-2,6-dichlorobenzenesulfonamide (**4f**).* Yellow solid, yield: 78% mp: 232−234 °C; ^{1}H NMR (δ ppm, DMSO-d$_6$, 300 MHz): 10.04 (s, 1H, sulfonamide, N−H), 8.66 (s, 1H, N−H); 8.17 (d, J = 9.0 Hz, 1H, CH, pyrimidine, Ar−H), 6.84−7.43 (m 10H, Ar−H), 6.59 (d, J = 9 Hz, 2H, NH$_2$); ^{13}C NMR (δ ppm, DMSO-d$_6$, 75 MHz): 173.58, 165.93, 162.31, 160.00, 159.94, 156.87, 154.36, 152.38, 151.04, 147.35, 144.94, 138.87, 135.87, 132.94, 131.87, 129.10, 128.93, 128.87, 127.31, 126.11, 125.26, 124.58, 124.38, 123.93, 117.31, 115.87.

*N-(3-(2-(6-Amino-1,4-dioxo-3,4-dihydrophthalazin-2(1H)-yl)-5-(2-chloropyrimidin-4-yl)thiazol-4-yl)-2-chlorophenyl)-2,6-dichlorobenzenesulfonamide (**4g**).* Pale-yellow solid, yield: 75% mp: 236−238 °C; ^{1}H NMR (δ ppm, DMSO-d_6, 300 MHz): 10.65 (s, 1H, sulfonamide, N−H), 9.49 (s, 1H, N−H), 8.19 (s, 1H, Ar−H), 8.11−8.14 (d, J = 9 Hz, 1H, CH, pyrimidine, Ar−H), 6.98−7.82 (m, 9H, Ar−H) 6.59 (s, 2H, NH$_2$); ^{13}C NMR (δ ppm, DMSO-d_6, 75 MHz): 172.92, 165.93, 162.31, 160.03, 159.92, 156.87, 154.36, 152.38, 151.04, 147.35, 144.95, 138.82, 135.81, 132.94, 131.83, 129.10, 128.87, 128.40, 127.33, 126.11, 125.26, 124.52, 124.37, 123.90, 117.36, 115.81.

*N-(3-(5-(2-Chloropyrimidin-4-yl)-2-(8-hydroxy-1,4-dioxo-3,4-dihydrophthalazin-2(1H)-yl)thiazol-4-yl)-2-chlorophenyl)-2,6-dichlorobenzenesulfonamide (**4h**).* Pale-yellow solid, yield: 86% mp: 252−254 °C; yield: 88% mp: 232−234 °C; ^{1}H NMR (δ ppm, DMSO-d$_6$, 300 MHz): 10.74 (s, NH, amide), 10.04 (s, 1H, OH), 8.66 (s, 1H, NH), 8.17 (d, J = 9.0 Hz, 1H, pyrimidine, Ar−H), 7.05−7.43 (m, 7H, Ar−H), 6.84−6.91 (m, 2H, Ar−H), 6.57 (d, J = 9.0 Hz, 1H, pyrimidine, Ar−H); ^{13}C NMR (δ ppm, DMSO-d$_6$, 75 MHz): 174.54, 166.04, 161.68, 160.66, 160.10, 159.82, 159.75, 158.20, 156.69, 154.15, 150.82, 147.17, 135.69, 132.24, 131.08, 130.20, 128.96, 128.67, 127.98, 127.69, 125.83, 125.08, 124.37, 123.13, 122.94, 120.01, 117.25.

*N-(3-(5-(2-Chloropyrimidin-4-yl)-2-(8-nitro-1,4-dioxo-3,4-dihydrophthalazin-2(1H)-yl)thiazol-4-yl)-2-chlorophenyl)-2,6-dichlorobenzenesulfonamide (**4i**).* Yellow solid, yield: 89% mp: 218−220 °C; ^{1}H NMR (δ ppm, DMSO-d$_6$, 300 MHz): 10.12 (s, 1H, sulfonamide NH); 8.67 (s, 1H, NH), 8.26 (d, J = 6.0 Hz, 1H, Pyrimidine, Ar−H), 7.00−7.70 (m, 9H, Ar−H), 6.73 (d, J = 9.0 Hz, 1H, Pyrimidine, Ar−H); ^{13}C NMR (δ ppm, DMSO-d$_6$, 75 MHz): 173.94, 165.75, 162.13, 159.82, 159.75, 156.69, 154.15, 150.82, 148.20, 147.17, 135.69, 133.93, 132.55, 131.08, 130.29, 128.96, 128.67, 127.98, 127.69, 127.02, 125.93, 125.08, 124.37, 124.20, 123.13, 122.94, 117.25.

*N-(3-(5-(2-Chloropyrimidin-4-yl)-2-(7-nitro-1,4-dioxo-3,4-dihydrophthalazin-2(1H)-yl)thiazol-4-yl)-2-chlorophenyl)-2,6-dichlorobenzenesulfonamide (**4j**).* Yellow solid, yield: 86% mp: 224−228 °C; ^{1}H NMR (δ ppm, DMSO-d$_6$, 300 MHz): 10.11 (s, 1H, sulfonamide, NH), 8.39 (s, 1H, NH), 8.29 (d, J = 9.0 Hz, 1H, Ar−H), 8.17 (d, J = 6.0 Hz, 1H, pyrimidine, Ar−H), 7.01−7.60, (m, 8H, Ar−H), 6.64 (d, J = 9.0 Hz, 1H, pyrimidine, Ar−H); ^{13}C NMR (δ ppm, DMSO-d$_6$, 75 MHz): 183.46, 165.67, 161.41, 160.59, 160.02, 159.75, 159.68, 156.61, 154.07, 151.45, 150.74, 147.09, 135.61, 133.86, 131.00, 130.21, 128.88, 128.60, 127.90, 127.61, 126.55, 125.00, 124.30, 124.12, 123.05, 122.87, 117.18.

*N-(3-(5-(2-Chloropyrimidin-4-yl)-2-(5,8-dioxo-5,6-dihydropyrido[2,3-d]pyridazin-7(8H)-yl)thiazol-4-yl)-2-chlorophenyl)-2,6-dichlorobenzenesulfonamide (**4k**).* Pale-yellow solid, yield: 78% mp: 224−226 °C; ^{1}H NMR (δ ppm, DMSO-d6, 300 MHz): 10.15 (s, 1H, amide NH), 8.76 (s, 1H, NH), 8.17 (d, J = 9 Hz, 1H, pyrimidine, Ar−H), 7.46−7.61 (m, 4H, Ar−H), 7.02−7.26 (m, 5H, Ar−H), 6.64 (d, J = 9 Hz, 1H, pyrimidine, Ar−H); ^{13}C NMR (δ ppm, DMSO-d$_6$, 75 MHz): 183.74, 165.93, 162.31, 160.00, 159.94, 156.87, 154.36, 152.38, 151.04, 147.35, 144.03, 138.10, 135.87, 132.10, 131.27, 129.10, 128.86, 128.16, 127.86, 126.11, 125.26, 124.58, 124.38, 123.31, 117.47, 115.45.

*N-(3-(5-(2-Chloropyrimidin-4-yl)-2-(3,6-dioxo-2,3-dihydropyridazin-1(6H)-yl)thiazol-4-yl)-2-chlorophenyl)-2,6-dichlorobenzenesulfonamide (**4l**).* Pale-yellow solid, yield: 92% mp: 194−196 °C; ^{1}H NMR (δ ppm, DMSO-d$_6$, 300 MHz): 10.06 (s, 1H, sulfonamide NH), 8.40 (s, 1H, NH), 8.30 (d, J = 6 Hz, 1H, Ar−H), 8.17 (d, J = 9 Hz, 1H, pyrimidine Ar−H), 6.91−7.49 (m, 8H, Ar−H), 6.64 (d, J = 9 Hz, 1H, pyrimidine Ar−H). ^{13}C NMR (δ ppm, DMSO-d$_6$, 75 MHz): 183.82,

https://doi.org/10.1021/acsomega.4c05587
ACS Omega 2024, 9, 38262−38271

166.38, 162.12, 160.94, 160.38, 160.10, 160.03, 156.96, 155.79, 154.43, 151.10, 147.45, 135.97, 132.56, 131.36, 131.21, 129.24, 128.95, 125.35, 124.65, 117.53, 115.54, 113.57.

*N-(3-(5-(2-Chloropyrimidin-4-yl)-2-(3,6-dioxotetrahydropyridazin-1(2H)-yl)thiazol-4-yl)-2-chlorophenyl)-2,6-dichlorobenzenesulfonamide (**4m**).* Pale-yellow solid, yield: 90% mp: 192−194 °C; ^{1}H NMR (δ ppm, DMSO-d_6, 300 MHz): 10.02 (s, 1H, sulfonamide NH), 8.39 (s, 1H, NH), 8.08 (d, J = 9.0 Hz, 1H, pyrimidine, Ar−H), 6.99−7.54 (m, 6H, Ar−H), 6.57 (d, J = 9.0 Hz, 1H, pyrimidine, Ar−H), 2.55 (s, 4H, tetrahydropyridazine-3,6-dione, CH_2); ^{13}C NMR (δ ppm, DMfSO-d_6, 75 MHz): 184.02, 161.14, 160.58, 160.30, 160.23, 157.16, 154.63, 151.30, 147.65, 136.17, 131.56, 129.44, 129.15, 128.46, 128.17, 125.55, 124.85, 124.67, 123.60, 123.42, 117.73, 28.49, 25.58.

*2,6-Dichloro-N-(2-chloro-3-(2-(4-(3-chloro-2-cyanobenzylidene)-1-oxo-3,4-dihydrophthalazin-2(1H)-yl)-5-(2-chloropyrimidin-4-yl)thiazol-4-yl)phenyl)benzenesulfonamide (**4n**).* Yellow solid, yield: 82% mp: 258−260 °C; ^{1}H NMR (δ ppm, DMSO-d_6, 300 MHz): 10.76 (s, 1H, sulfonamide NH), 9.27 (s, 1H, NH), 8.25 (s, 1H, C−H), 7.84−8.22 (m, 3H, pyrimidine Ar−H), 7.09−7.70 (m, 11H, Ar−H), 6.68 (d, J = 9 Hz, 1H, pyrimidine Ar−H); ^{13}C NMR (δ ppm, DMSO-d_6, 75 MHz): 183.72, 166.40, 161.67, 160.85, 160.28, 160.01, 159.94, 156.87, 154.33, 151.00, 147.35, 144.73, 141.09, 135.87, 134.12, 133.12, 132.74, 131.27, 129.14, 128.86, 128.16, 127.87, 126.86, 126.01, 125.26, 125.20, 124.56, 124.38, 123.31, 123.13, 121.90, 118.15, 117.44, 116.34, 113.17.

*2,6-Dichloro-N-(2-chloro-3-(5-(2-chloropyrimidin-4-yl)-2-(4-(2-cyanobenzylidene)-1-oxo-3,4-dihydrophthalazin-2(1H)-yl)thiazol-4-yl)phenyl)benzenesulfonamide (**4o**).* Yellow solid, yield: 78% mp: 261−263 °C; ^{1}H NMR (δ ppm, DMSO-d_6, 300 MHz): 10.65 (s, 1H, sulfonamide NH), 8.82 (s, 1H, NH), 8.11−8.19 (m, 2H, Ar−H), 7.73−7.82 (m, 3H, Ar−H, 1H, C−H), 6.98−7.56 (m, 11H, Ar−H), 6.57 (d, J = 9.0 Hz, 1H, pyrimidine Ar−H); ^{13}C NMR (δ ppm, DMSO-d6, 75 MHz): 183.71, 166.40, 160.85, 160.28, 160.01, 159.94, 156.87, 154.32, 151.00, 147.36, 145.10, 138.37, 135.86, 134.76, 133.13, 132.13, 131.47, 131.27, 131.11, 129.14, 128.86, 128.16, 127.87, 125.21, 124.56, 124.38, 123.31, 123.11, 122.12, 121.83, 120.85, 119.47, 117.44, 115.45, 113.47.

Preparation of the $NiFe_2O_4$ Catalyst. $NiFe_2O_4$ nanoparticles were synthesized via our previously reported sol−gel method and used in our earlier work.[37] The crystalline nature of the catalyst was confirmed through powder X-ray diffraction (XRD) analysis (can be seen in Supporting Information).

***In Silico* Molecular Docking Studies.** Molecular docking studies were conducted using the Schrödinger suite (Schrödinger, LLC), with protein−ligand interactions visualized via Maestro. The HSP82 and HSP90 crystal structures were sourced from the Protein Data Bank and prepared using the Protein Preparation Wizard. This process involved removing water molecules, adding missing hydrogens, assigning protonation states using PROPKA at pH 7.0, and minimizing the structure with the OPLS4 force field. Ligands were prepared using LigPrep by converting 2D structures to 3D, generating ionization states at pH 7.0, producing tautomers and stereoisomers, and minimizing with the OPLS4 force field. The receptor grid was created using the centroid of the cocrystallized ligand as the binding site reference, with grid box dimensions set to 20 × 20 × 20 Å. Docking was performed in Glide's Extra Precision (XP) mode, generating up to 10 poses per ligand and scoring them with the Glide Score. The best poses were selected based on the lowest Glide Score and visual inspection of binding interactions.

Cell Viability Assay. Cell lines for human breast adenocarcinoma (MCF-7) and epithelial cervix adenocarcinoma (HeLa) were obtained from the National Centre for Cell Science (NCCS), Pune, India. Every cell line was kept in Dulbecco's modified Eagle's medium (DMEM high glucose), which was enhanced with 1% penicillin/streptomycin (100 U/mL; 0.1 mg/mL) and 10% fetal bovine serum (FBS). At a density of 7 × 103 cells per well, the cells were seeded in triplicate onto 96-well plates and allowed to adhere for 24 h. Different drug concentrations were applied to the adherent cells for a duration of 48 h. At the onset of the treatment period, the cell viability was assessed by the 3-(4,5-dimethylthiazol-2-yl)2,5-diphenyltetrazolium bromide (MTT) assay (HiMedia, Mumbai, India).[38] Fractional cell survival was measured by taking absorbance at 570 nm (Infinite 200 PRO, Tecan, Switzerland) and subtracting the background measurement at 650 nm. The data were normalized by taking the absorbance of untreated cells (i.e., control) as 100%. The IC_{50} values were calculated by using nonlinear curve regression in Prism, version 5.01 (GraphPad Software Inc., San Diego, California, USA), and presented as the mean ± SD of three independent experiments. Statistical significance of differences was calculated using the two-way analysis of variance (ANOVA) and Tukey's post hoc test for pairwise comparisons. Statistically significant values were taken as *p < 0.05, **p < 0.01, ***p < 0.001, and ****p < 0.0001.

RESULTS AND DISCUSSION

Initially, we tried to synthesize thiazolyl-phthalazine (**4a**) from compound (**1**) with thiosemicabazide (**2**) and phthalic anhydride (**3a**) in a model study (Scheme 2). Initially, the

Scheme 2. Facile Nano-$NiFe_2O_4$-Catalyzed Synthesis of 2,6-Dichloro-*N*-(2-chloro-3-(5-(2-chloropyrimidin-4-yl)-2-(1,4-dioxo-3,4-dihydrophthalazin-2(1*H*)-yl)thiazol-4-yl)phenyl)benzenesulfonamide

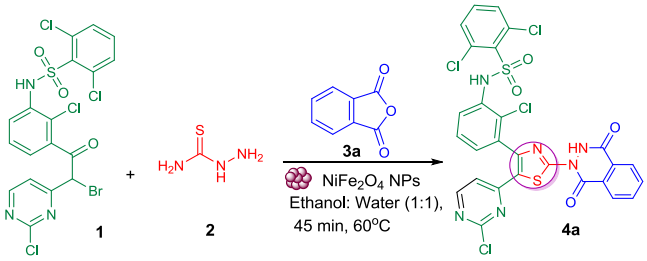

reaction was conducted in refluxing H_2O, but only 32% yields of **4a** were obtained (Table 1, entry 1). Further on, we have observed that the yield of **4a** could be improved to 55% by using ethanol as a solvent (Table 1, entry 2). Subsequently, we examined the mixed ethanol/water (EtOH/H_2O) in (1:1) proportion without any catalyst and we observed that the yield of **4a** was increased to 73% (Table 1, entry 3). Then, we tried to improve the yields of targeted compound by using aqueous ethanol (1:1) with different amounts of nano-$NiFe_2O_4$ catalyst (Table 1, entries 4−6). Among which, the best result was received from aqueous ethanol and 5 mg of nano-$NiFe_2O_4$ catalyst, delivering **4a** in 90% yield (Table 1, entry 4) (Scheme 2). As a comparison to this, the reaction conducted in DMF,

https://doi.org/10.1021/acsomega.4c05587
ACS Omega 2024, 9, 38262−38271

Table 1. Optimization of Reaction Conditions[a]

entry	catalysts	solvent	temp. (°C)	time	yield (%)[b]
1	no catalyst	H_2O	100	5 h	32
2	no catalyst	EtOH	75	5 h	55
3	no catalyst	EtOH: H_2O (1:1)	75	5 h	73
4[c]	$NiFe_2O_4$ NPs	EtOH: H_2O (1:1)	75	1h	90
5[d]	$NiFe_2O_4$ NPs	EtOH: H_2O (1:1)	75	1h	83
6[e]	$NiFe_2O_4$ NPs	EtOH: H_2O (1:1)	75	1h	92
7[f]	$NiFe_2O_4$ NPs	EtOH: H_2O (1:1)	75	45 min	92
8	$NiFe_2O_4$ NPs	DMF	75	2 h	70
9	$NiFe_2O_4$ NPs	CH_3CN	75	2 h	68
10	$NiFe_2O_4$ NPs	$C_6H_5-CH_3$	75	2 h	67
11	$ZnFe_2O_4$ NPs	EtOH: H_2O (1:1)	75	2 h	72

[a]Reactions were carried out among 3-(2-bromo-2-(2-chloropyrimidin-4-yl)acetyl)-2-chlorophenyl-2,6-dichlorobenzenesulfonamide (1 mmol), thiosemicarbazide (1 mmol), and phthalic anhydride (1 mmol) in the presence of ethanol and 5 mg of catalysts. [b]Yield of isolated product. [c]5 mg of $NiFe_2O_4$. [d]3 mg of $NiFe_2O_4$. [e]7 mg of $NiFe_2O_4$. [f]10 mg of $NiFe_2O_4$ was refluxed.

CH_3CN, and toluene all gave poorer results (Table 1, entries 8−10).

To establish the importance of nano-$NiFe_2O_4$, we have carried out the same reaction with the $ZnFe_2O_4$ catalyst. It was observed that $ZnFe_2O_4$ was found to be inactive in the reaction (entry 11, Table 1). It was also observed that increasing or decreasing the amount of catalyst affects the yields (10 mg, entry 6, Table 1; 3 mg, entry 5, Table 1).

After optimization of the reaction conditions to delineate this approach, the present methodology was evaluated with a variety of anhydrides **3b−3o** in the presence of nano-$NiFe_2O_4$ under similar conditions. As we have expected, the reaction conditions worked well for all the anhydrides, resulting in different phthalazines, pyradizines, and pyridopyridiazines **4a−4o** in high yields (Table 2). Therefore, the above results suggest that the one-pot, three-component cyclocondensation reaction proceeded smoothly. This research could lead to intriguing chemistry involving novel methodologies. A notable feature of the synthesis is its ability to produce various heteroatom bonds at a time, such as one C−S and three C−N in a one-pot hetero cyclization process, all without producing any other products. The $NiFe_2O_4$ NPs can be involved in the activation of thiosemicarbazide (**2**). The thiosemicarbazide reacts with (*N*-(3-(2-bromo-2-(2-chloropyrimidin-4-yl)acetyl)-2-chlorophenyl)-2,6-dichlorobenzenesulfonamide to give uncyclized thio-ketone with the removal of HBr, which is further cyclized by removal of water molecules and produces an thiazolo-hydrazinyl intermediate. Afterward, it undergoes a reaction with phthalic anhydride to produce the final product **4a** in excellent yields. These results can be corroborated with

Table 2. Substrate Scope of Thiazole Scaffolds Using $NiFe_2O_4$ Nanoparticles (4a−4o)[a]

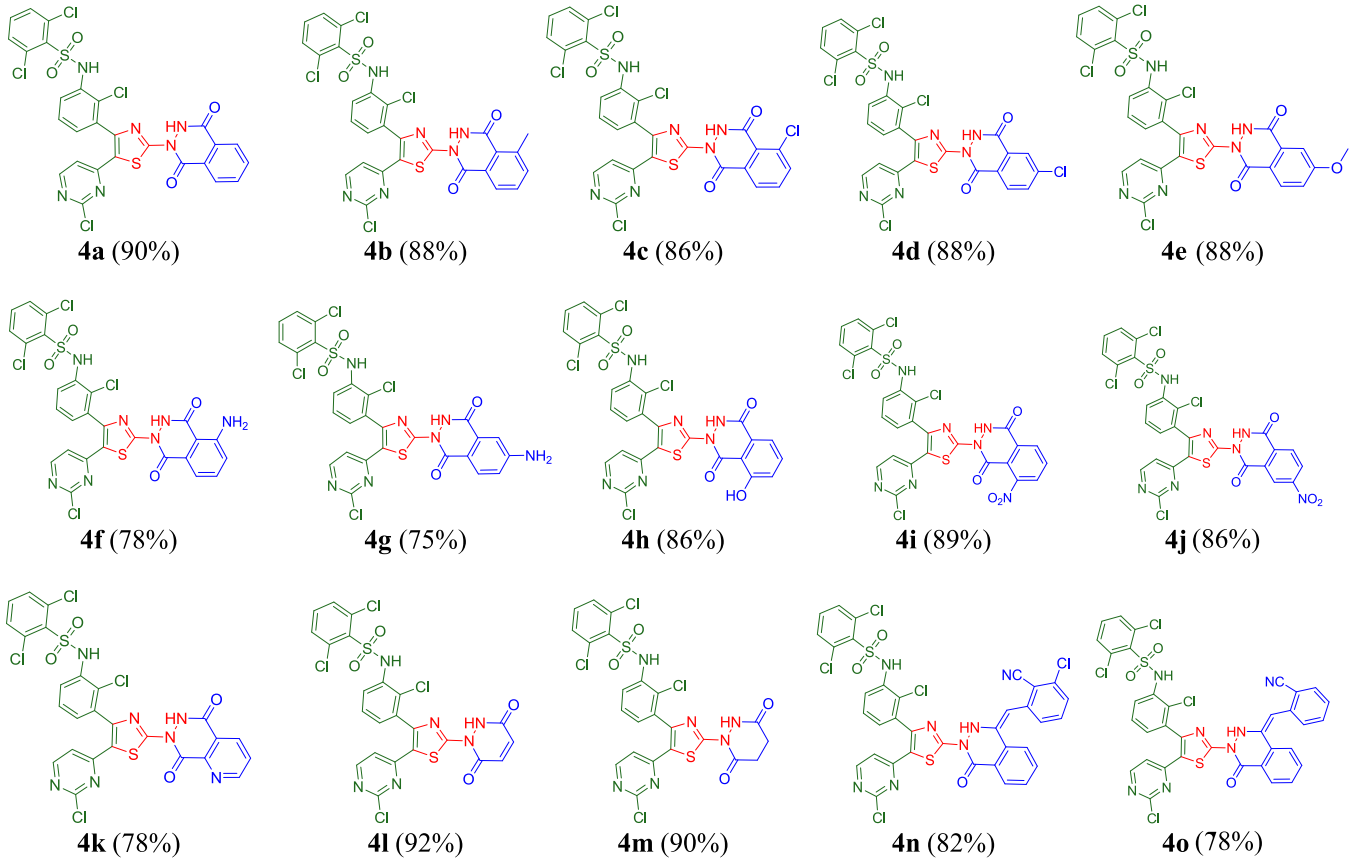

[a]Reactions were carried out for 3-(2-bromo-2-(2-chloropyrimidin-4-yl)acetyl)-2-chlorophenyl-2,6-dichlorobenzenesulfonamide (1 mmol), thiosemicarbazide (1 mmol), and various anhydrides (1 mmol) in the presence of ethanol:water and 5 mg of nano-$NiFe_2O_4$ catalyst.

https://doi.org/10.1021/acsomega.4c05587
ACS Omega 2024, 9, 38262−38271

the recently synthesized thiazole scaffolds using the TCsSB catalyst, yielding 87% under ultrasound irradiation in ethanol.[39] Conversely, our method entails a one-pot, three-component synthesis employing $NiFe_2O_4$ nanoparticles as catalysts, achieving a superior 90% yield of thiazole scaffolds within 60 min under reflux conditions at 75 °C in an ethanol−water solvent system, utilizing only 5 mg of catalyst a notably minimal amount.

Furthermore, our catalyst demonstrates remarkable reusability. Similarly, Sadgar et al. synthesized thiazoles using graphene as a catalyst and reported 93% yields in the presence of toluene.[40] Nevertheless, that procedure involves a hazardous solvent when compared to our procedure. The chemical structures of final compounds were confirmed by ^{1}H NMR, ^{13}C NMR, and mass spectrometry. For example, the ^{1}H NMR spectra of compound **4a** showed two doublets at δ 6.60−6.63 and 8.20−8.23 for pyrimidine C−H protons and another two singlets appeared at δ 8.67 and δ 10.08 for NH and N−H (near to sulfonyl) protons, respectively. As shown in ^{13}C NMR spectral data, sharp peaks appeared at δ 160.51, 163.96, and 173.53 ppm for carbonyl carbon signals of the phthalazinone and thiazole (C═N) carbon, respectively. Thus, the remaining spectral data confirm the structures of newly prepared compounds (**4a**−**4o**).

Nano-$NiFe_2O_4$ Catalyst Reusability Study. The reusability test has been performed after completion of the reaction to check the activity of the catalyst.

The nano-$NiFe_2O_4$ recyclability was examined under standard conditions for **4a** compound synthesis (Table 1) as a model reaction. An external magnet was used to recover the $NiFe_2O_4$ NP catalyst from the reaction mixture and thoroughly washed with hot distilled water and ethanol, respectively (four times). After being dried in a hot air oven, the catalyst was reused for the remaining reactions with the same reaction conditions. It has been determined that the catalyst, nano-$NiFe_2O_4$, exhibits no degradation after over 10 catalytic cycles. The outcomes of this reusability are presented in Figure 2

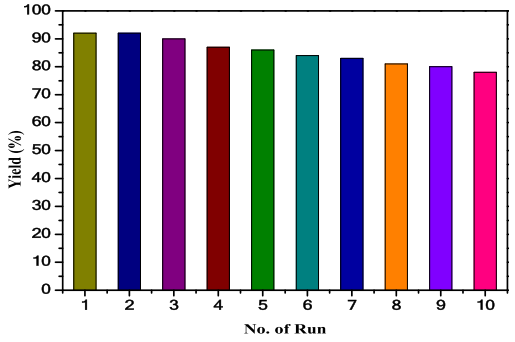

Figure 2. Recyclability of the nano-$NiFe_2O_4$ catalyst for the synthesis of **4a**.

***In Silico* Molecular Docking Studies.** *In silico* docking studies were conducted to evaluate the binding affinities of various ligands against Hsp82 from *Saccharomyces cerevisiae* and Hsp90 from *Homo sapiens*, both expressed in *E. coli* (Figure 3). The *in silico* docking studies for the Hsp82 protein revealed varying binding affinities and interaction profiles among the tested ligands, with several outperforming the reference drug erlotinib. Erlotinib demonstrated a docking score of −6.27 kcal/mol, forming six hydrogen bonds and four

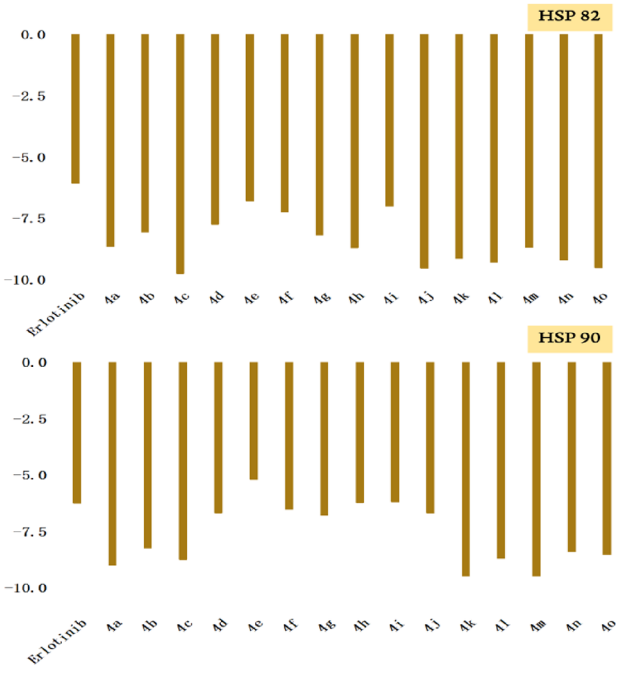

Figure 3. Comparative interaction analysis with Hsp82 and Hsp90.

hydrophobic interactions with residues Asp 175, Thr 176, Gly 177, Glu 178, Lys 185, His 189, Asp 86, Thr 88, Ile 187, Asn 51, and Lys 58. Among the ligands, **4k** and **4m** exhibited the highest binding affinities, both with a docking score of −9.5 kcal/mol. Ligand **4k** formed three hydrogen bonds and two hydrophobic interactions with residues Lys 208, Ile 214, Val 207, and Ile 218. Similarly, **4n** interacted with the same residues, emphasizing its strong binding capacity. Ligands **4a**, **4c**, **4l**, and **4n** also displayed substantial binding affinities with docking scores of −9.01, −8.75, −8.71, and −8.41 kcal/mol, respectively. These ligands formed multiple hydrogen bonds and hydrophobic interactions with key residues such as Lys 208, Ile 214, Gln 212, and Leu 220, highlighting their potential as effective Hsp82 inhibitors.

For the Hsp90 protein, erlotinib showed a docking score of −6.08 kcal/mol, forming three hydrogen bonds, four hydrophobic interactions, and one π-stacking interaction with residues Ser 36, Phe 200, Arg 32, Glu 199, and Phe 200. The ligands demonstrated significantly lower docking scores, indicating stronger binding affinities. Ligands **4c**, **4j**, **4o**, and **4l** also showed excellent binding affinities with scores of −9.76, −9.55, −9.53, and −9.31 kcal/mol, respectively. These ligands were engaged in multiple hydrogen bonds, hydrophobic interactions, and additional π−cation and halogen bonds with residues Lys 195, Val 201, Tyr 203, Ile 205, Asn 37, Asn 91, Lys 98, Gly 121, Gly 123, Phe 124, Ile 205, Leu 207, Val 201, Val 209, and Asn 92. Other ligands, such as **4k** (−9.14 kcal/mol), **4n** (−9.21 kcal/mol), and **4m** (−8.7 kcal/mol), also demonstrated strong binding affinities, forming various interactions with key residues, indicating their potential effectiveness as Hsp90 inhibitors.

Overall, the *in silico* docking studies suggest that the synthesized ligands, particularly **4c**, **4j**, **4k**, **4l**, **4m**, and **4o**, exhibit superior binding affinities and interaction profiles compared to erlotinib for both Hsp82 and Hsp90 proteins. These ligands form multiple stable interactions with crucial residues, underscoring their potential as potent inhibitors.

https://doi.org/10.1021/acsomega.4c05587
ACS Omega 2024, 9, 38262−38271

ADME Analysis. The ADME analysis of the tested ligands reveals distinct properties, with respect to their interaction with various CYP450 enzymes and other pharmacokinetic parameters. Among the ligands, **4b**, **4c**, **4d**, and **4g** are nonsubstrates for CYP450 2C9, 2D6, and 3A4 while **4i**, **4j**, **4l**, and **4m** are noninhibitors of these enzymes. Ligands **4o** are identified as an inhibitor of both CYP450 2C9 and 3A4, indicating potential drug−drug interactions. For CYP450 inhibition, ligands **4c** and **4i** inhibit CYP450 1A2 while **4c**, **4j**, and **4n** inhibit CYP450 2C19. High CYP inhibitory promiscuity is observed in **4c**, **4j**, and **4n**, suggesting a higher likelihood of interactions with multiple CYP450 enzymes.

Blood−brain barrier (BBB) permeability and human intestinal absorption (HIA) probabilities show that most ligands, except **4d** and **4g**, have moderate to high BBB permeability and excellent HIA probabilities. Ligand **4n** exhibits the highest Caco-2 permeability, indicating good intestinal absorption. In terms of toxicity, **4b**, **4d**, and **4g** are identified as toxic in the AMES test, with **4c** being a potential carcinogen. Overall, ligands **4n**, **4j**, **4l**, **4m**, and **4o** exhibit favorable ADME profiles with nontoxicity, noncarcinogenicity, high HIA, and low CYP inhibitory promiscuity, making them promising candidates for further development.

Biological Studies. *In Vitro Cytotoxic Activity.* In a comparative study, newly synthesized compounds (**4a**−**4o**) and the well-known kinase inhibitor drug erlotinib were assessed for their in vitro anticancer activity against three human cancer cell lines A375, HeLa, and MCF-7, using the standard MTT assay (Figure 4).

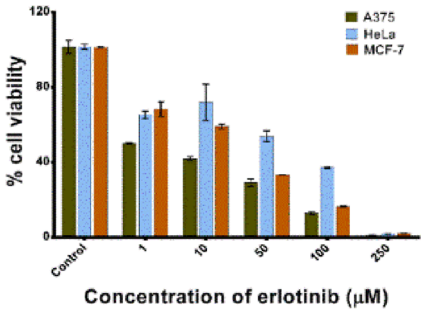

Figure 4. Cell viability assay on A375, MCF-7, and Hela cells with the reference drug erlotinib after dose-dependent treatment.

The results from the cell viability assay revealed that compounds **4j**, **4k**, **4m**, **4n**, and **4o** exhibited potent anticancer activity at a concentration of 1 μM against the tested cell lines. Particularly, compound **4n** demonstrated significant activity against all three cell lines: HeLa, A375, and MCF-7 (Figure 5).

The IC_{50} values were evaluated on the basis of preliminary bioassay results to examine the potential anticancer activities. The IC_{50} values of the final compounds are given in Table 3 and Figure 6.

As presented in Table 3, the cytotoxicity of synthesized compounds was evaluated against three cancer cell lines A375, HeLa, and MCF-7 using IC_{50} values (μM) as the metric and compared to the reference drug erlotinib. The IC_{50} values of 15 compounds were evaluated against three cancer cell lines: A375, HeLa, and MCF-7. For the A375 cell line, the five compounds with the lowest IC_{50} values were **4n** (0.87 ± 0.31 μM), **4k** (1.45 ± 0.12 μM), **4o** (1.72 ± 0.04 μM), **4l** (2.81 ± 0.96 μM), and **4m** (2.96 ± 2.01 μM). In HeLa cells, the most

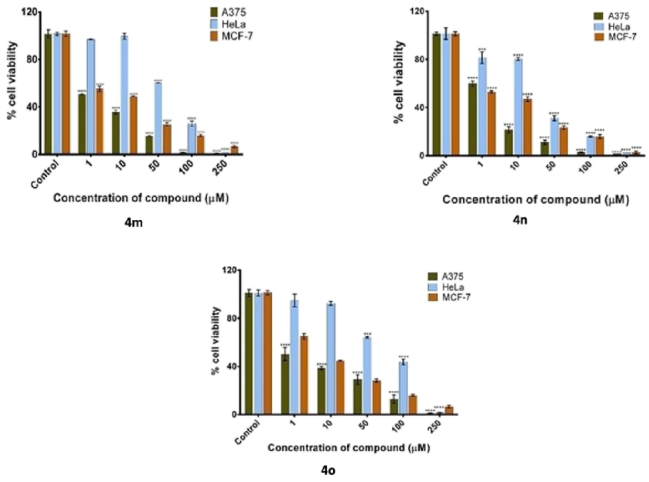

Figure 5. Cell viability percentage of **4m**, **4n**, and **4o** compounds. The anticancer activity of compounds was confirmed by the dose-dependent decrease in cell viability. *p < 0.05, **p < 0.01, ***p < 0.001, and ****p < 0.0001 were taken as statistically significant values.

Table 3. *In Vitro* Cytotoxicity of Compounds 4a−4o against Different Cancer Cell Lines by Using the MTT Assay

	IC_{50} values in μM[a]		
compound	A375	HeLa	MCF-7
4a	6.03 ± 0.41	22.37 ± 1.87	15.24 ± 2.22
4b	15.37 ± 2.78	NA[b]	NA
4c	2.96 ± 2.01	28.1 ± 0.82	8.8 ± 1.21
4d	3.17 ± 1.76	NA	12.59 ± 0.63
4e	5.30 ± 0.86	18.6 ± 0.15	3.9 ± 0.14
4f	7.37 ± 0.13	16.67 ± 0.12	8.26 ± 0.38
4g	4.30 ± 0.86	2.8 ± 2.13	6.9 ± 0.14
4h	11.42 ± 1.26	NA	21.96 ± 2.06
4i	4.30 ± 0.86	22.6 ± 2.15	9.69 ± 0.14
4j	6.67 ± 0.21	13.67 ± 0.15	9.22 ± 0.32
4k	1.45 ± 0.12	18.89 ± 0.31	7.79 ± 0.16
4l	2.81 ± 0.96	19.14 ± 0.22	11.52 ± 0.88
4m	2.96 ± 2.01	27.1 ± 0.82	8.89 ± 1.21
4n	0.87 ± 0.31	1.38 ± 1.24	1.13 ± 0.96
4o	1.72 ± 0.04	15.61 ± 0.35	8.45 ± 0.18
erlotinib[c]	3.60	41.80	15.55

[a]IC_{50}: After 48 h of drug exposure, the concentration of compound inhibits 50% cell growth, as determined by the MTT assay. Every test was run at least three times, and the results are given as the average values ± standard deviation. [b]NA: Compound shows IC_{50} value >50 μM/mL. [c]Erlotinib as a reference drug.

potent compounds were **4n** (1.38 ± 1.24 μM), **4g** (2.8 ± 2.13 μM), **4j** (13.67 ± 0.15 μM), **4o** (15.61 ± 0.35 μM), and **4f** (16.67 ± 0.12 μM). For the MCF-7 cell line, the most effective compounds were **4n** (1.13 ± 0.96 μM), **4e** (3.9 ± 0.14 μM), **4g** (6.9 ± 0.14 μM), **4k** (7.79 ± 0.16 μM), and **4f** (8.26 ± 0.38 μM). Overall, compound **4n** demonstrated the highest efficacy across all tested cell lines, whereas compound **4b** was the least efficient, showing no activity (NA) against HeLa and MCF-7 cell lines. The reference compound erlotinib exhibited IC_{50} values of 3.60 μM for A375, 41.80 μM for HeLa, and 15.55 μM for MCF-7, indicating that compound **4n** outperformed erlotinib in terms of potency.

Structure−Activity Relationship. The structure−activity relationship (SAR) analysis of the evaluated compounds

https://doi.org/10.1021/acsomega.4c05587
ACS Omega 2024, 9, 38262−38271

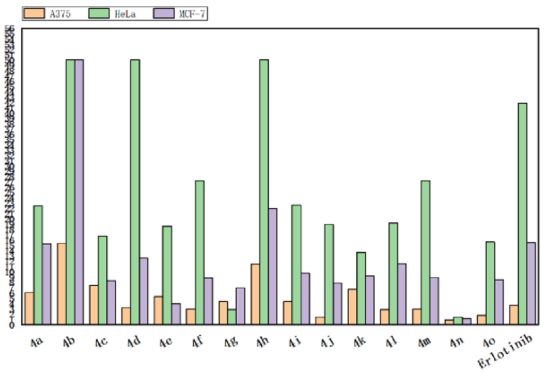

Figure 6. Cell viability assay of all the test ligands on A375, MCF-7, and Hela cells with the reference drug erlotinib.

reveals distinct trends based on the substituents and their positions in the core structure. Compounds **4n** and **4o**, which have a cyano substituent at the 2 and 3 positions, respectively, show the highest potency across all cell lines, suggesting that the presence of a cyano group significantly enhances activity. Compounds **4k** and **4e**, with methoxy and dioxopiperidine substituents, also demonstrate notable activity particularly in the A375 and MCF-7 cell lines. Compound **4g**, with an amino group at the 6-position, shows considerable activity, indicating that amino substitutions can positively impact efficacy. In contrast, compounds with nitro groups (**4i** and **4j**) and bulky groups (**4b**, **4d**, and **4h**) generally display higher IC_{50} values, suggesting lower activity. The presence of halogen atoms, such as chlorine, across all compounds indicates that these substituents might be crucial for maintaining a baseline level of activity. Overall, the most efficient compounds (**4n** and **4o**) benefit from cyano and benzylidene substitutions at strategic positions, highlighting their critical role in enhancing anticancer activity.

The in vitro cytotoxicity analysis, in silico molecular docking studies, and ADME properties collectively provide a comprehensive evaluation of the novel thiazole derivatives (**4a**−**4o**) synthesized in this study. The cytotoxicity analysis demonstrated that compound **4n** exhibited the most potent anticancer activity across all tested cell lines (A375, HeLa, and MCF-7), outperforming the reference drug erlotinib with significantly lower IC_{50} values. This finding is corroborated by the in silico docking studies, where **4n**, along with compounds **4k**, **4m**, **4c**, **4j**, **4o**, and **4l**, displayed superior binding affinities and interaction profiles compared to erlotinib against both Hsp82 and Hsp90 proteins. The high binding affinity of these ligands, particularly **4n**, is reflected in their ability to form multiple stable interactions with crucial residues, underscoring their potential as potent inhibitors. The ADME analysis further supports the potential of these compounds, especially **4n**, by highlighting their favorable pharmacokinetic profiles. Compound **4n**, along with **4j**, **4l**, **4m**, and **4o**, exhibited nontoxicity, noncarcinogenicity, high HIA (HIA), and low CYP inhibitory promiscuity. These properties suggest a reduced likelihood of adverse drug−drug interactions and good bioavailability, making them promising candidates for further development. The SAR analysis revealed that specific substituents, such as cyano and benzylidene groups, play a crucial role in enhancing the anticancer activity. Compounds **4n** and **4o**, which possess these substituents at strategic positions, consistently showed high potency across all cell lines. Conversely, compounds with nitro groups and bulky substituents generally exhibited lower activity, indicating that the nature and position of substituents significantly impact the efficacy of these compounds. The correlation between these analyses underscores the importance of strategic structural modifications to enhance biological activity, binding affinity, and favorable pharmacokinetic properties, ultimately leading to the identification of potent anticancer agents like compound **4n**.

CONCLUSIONS

In conclusion, the green one-pot multicomponent synthesis strategy successfully generated a series of novel thiazole derivatives (**4a**−**4o**) with promising anticancer properties. Among these, compound **4n** emerged as the most potent across A375, HeLa, and MCF-7 cancer cell lines, significantly outperforming the reference drug erlotinib. *In silico* docking studies underscored the strong binding affinities of several ligands, particularly **4k**, **4m**, **4c**, **4j**, **4o**, and **4l**, to Hsp82 and Hsp90 proteins. Compound **4n** showed a higher binding capacity for Hsp82. The ADME analysis indicated that compounds **4n**, **4j**, **4l**, **4m**, and **4o** possessed favorable pharmacokinetic profiles, with nontoxicity and high HIA. SAR analysis highlighted the importance of cyano and benzylidene substitutions in enhancing anticancer activity. The synthesized compounds, especially **4n**, demonstrate significant potential as effective anticancer agents, warranting further investigation and development.

ASSOCIATED CONTENT

Supporting Information

The Supporting Information is available free of charge at https://pubs.acs.org/doi/10.1021/acsomega.4c05587.

Data of NMR spectra of synthesized compounds **4a**−**4o**, molecular docking analysis, and anticancer studies (PDF)

AUTHOR INFORMATION

Corresponding Authors

Satish Gudala − *Department of Chemistry, National Institute of Technology, Raipur, Chhattisgarh 492010, India; Key Laboratory of Green Catalysis and Reaction Engineering of Haikou, College of Chemistry and Chemical Engineering, Hainan University, Haikou 570228, People's Republic of China*; Email: satish.orgchem@gmail.com

Archi Sharma − *Department of Chemistry, Vardhman College of Engineering, Hyderabad, Telangana 500085, India*; Email: sharmaarchizenith@gmail.com

Santhosh Penta − *Department of Chemistry, National Institute of Technology, Raipur, Chhattisgarh 492010, India; Department of Chemistry, National Institute of Technology, Warangal, Telangana 506004, India*; Email: santhoshpenta07@gmail.com

Jianxin Yang − *Key Laboratory of Green Catalysis and Reaction Engineering of Haikou, College of Chemistry and Chemical Engineering, Hainan University, Haikou 570228, People's Republic of China*; orcid.org/0000-0002-0082-227X; Email: yangjxmail@hainanu.edu.cn

Authors

Aruna Lankada − *Department of Biosciences and Bioengineering, Indian Institute of Technology, Guwahati 781039, India*

https://doi.org/10.1021/acsomega.4c05587
ACS Omega 2024, 9, 38262−38271

Ruotong Liu − *Key Laboratory of Green Catalysis and Reaction Engineering of Haikou, College of Chemistry and Chemical Engineering, Hainan University, Haikou 570228, People's Republic of China*

Anubhuti Jha − *Department of Biotechnology, St. Thomas College, Hemchand Yadav University, Durg, Chhattisgarh 490006, India*

Owias Iqbal Dar − *Key Laboratory of Ministry of Education for Advance Materials in Tropical Island Resources, College of Chemistry and Chemical Engineering, Hainan University, Haikou 570228, People's Republic of China*

Complete contact information is available at: https://pubs.acs.org/10.1021/acsomega.4c05587

Author Contributions

S.G.: data curation, conducting of all experiments, analysis of the data, writing—original draft. A.S.: data curation, analyzing of the data, writing—original draft. S.P.: conceptualization, lab facility, editing and supervision. J.Y.: conceptualization, funding, lab facility, reviewing of the data and editing. A.L.V.: anticancer and ADME studies. A.J.: molecular docking and anticancer studies. R.L.: molecular docking studies. O.I.D.: molecular docking studies and biological data evaluation. All authors have read and agreed to the published version of the manuscript.

Notes

The authors declare no competing financial interest.

■ ACKNOWLEDGMENTS

The authors are thankful for the Hainan Provincial Natural Science Foundation of China (Grant No. 221RC1016), the National Natural Science Foundation of China (Grant No. 52063011), and the Sanya Yazhouwan Science and Technology City Administration Bureau (SKJC-2020-01-004).

■ ABBREVIATIONS

SAR: structure−activity relationship; ADME: absorption, distribution, metabolism, and excretion; HSP: heat shock proteins; MCR: multicomponent reaction

■ REFERENCES

(1) WHO *Cancer* https://www.who.int/news-room/fact-sheets/detail/cancer (accessed 2024−06−07).

(2) Sung, H.; Ferlay, J.; Siegel, R. L.; Laversanne, M.; Soerjomataram, I.; Jemal, A.; Bray, F. Global Cancer Statistics 2020: GLOBOCAN Estimates of Incidence and Mortality Worldwide for 36 Cancers in 185 Countries. *CA. Cancer J. Clin.* **2021**, *71* (3), 209−249.

(3) Ferlay, J.; Colombet, M.; Soerjomataram, I.; Parkin, D. M.; Piñeros, M.; Znaor, A.; Bray, F. Cancer Statistics for the Year 2020: An Overview. *Int. J. Cancer* **2021**, *149* (4), 778−789.

(4) Hamilton, W. Cancer Diagnosis in Primary Care. *Br. J. Gen. Pract.* **2010**, *60* (571), 121−128.

(5) Kumar, A.; Singh, A. K.; Singh, H.; Vijayan, V.; Kumar, D.; Naik, J.; Thareja, S.; Yadav, J. P.; Pathak, P.; Grishina, M.; Verma, A.; Khalilullah, H.; Jaremko, M.; Emwas, A.-H.; Kumar, P. Nitrogen Containing Heterocycles as Anticancer Agents: A Medicinal Chemistry Perspective. *Pharmaceuticals* **2023**, *16* (2), 299.

(6) Pola, S. Significance of Thiazole-Based Heterocycles for Bioactive Systems. In *Scope of Selective Heterocycles from Organic and Pharmaceutical Perspective*; Varala, R., Ed.; InTech: 2016 .

(7) Farghaly, T. A.; Alsaedi, A. M. R.; Alenazi, N. A.; Harras, M. F. Anti-Viral Activity of Thiazole Derivatives: An Updated Patent Review. *Expert Opin. Ther. Pat.* **2022**, *32* (7), 791−815.

(8) Santos, N. D. F. N.; Junior, N. D. S. B.; De Oliveira, J. F.; Duarte, D. M. F. A.; Dos Santos Soares, J. C.; Marques, D. S. C.; Da Silva Santos, A. C.; Nogueira, F.; Pereira, V. R. A.; De Lima, M. C. A.; Da Cruz Filho, I. J. Synthesis, Characterization, Antioxidant and Antiparasitic Activities New Naphthyl-Thiazole Derivatives. *Exp. Parasitol.* **2023**, *248*, No. 108498.

(9) Biernasiuk, A.; Berecka-Rycerz, A.; Gumieniczek, A.; Malm, M.; Łączkowski, K. Z.; Szymańska, J.; Malm, A. The Newly Synthesized Thiazole Derivatives as Potential Antifungal Compounds against Candida Albicans. *Appl. Microbiol. Biotechnol.* **2021**, *105* (16−17), 6355−6367.

(10) Laboud, Y. N.; Zahran, D.; Hassaneen, H. M.; Elwahy, A. H. M.; Saleh, F. M. Synthesis and Anti-Bacterial Evaluation of Novel Scaffolds Based on Bis-Thiazole or Bis-1,3,4-Thiadiazole Linked to Thieno[2,3- *b*]Thiophene as New Hybrid Molecules. *ChemistrySelect* **2024**, *9* (14), No. e202400045.

(11) Agili, F. Novel Thiazole Derivatives Containing Imidazole and Furan Scaffold: Design, Synthesis, Molecular Docking, Antibacterial, and Antioxidant Evaluation. *Molecules* **2024**, *29* (7), 1491.

(12) Fadaly, W. A. A.; Zidan, T. H.; Kahk, N. M.; Mohamed, F. E. A.; Abdelhakeem, M. M.; Khalil, R. G.; Nemr, M. T. M. New Pyrazolyl-Thiazolidinone/Thiazole Derivatives as Celecoxib/Dasatinib Analogues with Selective COX-2, HER-2 and EGFR Inhibitory Effects: Design, Synthesis, Anti-Inflammatory/Anti-Proliferative Activities, Apoptosis, Molecular Modelling and ADME Studies. *J. Enzyme Inhib. Med. Chem.* **2023**, *38* (1), 2281262.

(13) Berredjem, M.; Bouchareb, F.; Djouad, S.; Bouasla, R.; Bahadi, R.; Redjemia, R.; Boussaker, M.; Dekir, A. Recent Progress in Synthesis of Sulfonamides and N-Acylsulfonamides, Biological Applications and Their Structure-Activity Relationship (SAR) Studies. *ChemistrySelect* **2023**, *8* (35), No. e202301859.

(14) Bhatnagar, A.; Pemawat, G. Functionalized Pyrimidines: Synthetic Approaches and Biological Activities. A Review. *Org. Prep. Proced. Int.* **2024**, *56* (1), 1−18.

(15) Hassan, G. S. Synthesis and Antitumor Activity of Certain New Thiazolo[2,3-b]Quinazoline and Thiazolo[3,2-a]Pyrimidine Analogs. *Med. Chem. Res.* **2014**, *23* (1), 388−401.

(16) Al-Omary, F. A. M.; Hassan, G. S.; El-Messery, S. M.; El-Subbagh, H. I. Substituted thiazoles V. Synthesis and Antitumor Activity of Novel Thiazolo[2,3-b]Quinazoline and Pyrido[4,3-d]-Thiazolo[3,2-a]Pyrimidine Analogues. *Eur. J. Med. Chem.* **2012**, *47*, 65−72.

(17) Rana, R.; Kumar, N.; Gulati, H. K.; Sharma, A.; Khanna, A.; Pooja; Badhwar, R.; Dhir, M.; Jyoti; Singh, J. V.; Bedi, P. M. S. A Comprehensive Review on Thiazole Based Conjugates as Anti-Cancer Agents. *J. Mol. Struct.* **2023**, *1292*, No. 136194.

(18) Mondru, A. K.; Wilkinson, B.; Aljasir, M. A.; Alrumayh, A.; Greaves, G.; Emmett, M.; Albohairi, S.; Pritchard-Jones, R.; Cross, M. J. The ERK5 Pathway in BRAFV600E Melanoma Cells Plays a Role in Development of Acquired Resistance to Dabrafenib but Not Vemurafenib. *FEBS Lett.* **2024**, 2011.

(19) Giraulo, C.; Orlando, L.; Morretta, E.; Voli, A.; Plaitano, P.; Cicala, C.; Potaptschuk, E.; Müller, C. E.; Tosco, A.; Monti, M. C.; Morello, S. High Levels of Soluble CD73 Unveil Resistance to BRAF Inhibitors in Melanoma Cells. *Biomed. Pharmacother.* **2024**, *177*, No. 117033.

(20) Baghdadi, R. A.; Abdalla, A. N.; Abourehab, M. A. S.; Tulbah, A. S. Evaluation of the Effects of a Dasatinib-Containing, Self-Emulsifying, Drug Delivery System on HT29 and SW420 Human Colorectal Carcinoma Cells, and MCF7 Human Breast Adenocarcinoma Cells. *J. Taibah Univ. Med. Sci.* **2024**, *19* (4), 806−815.

(21) Lamey, C. A.; Moussa, N.; Helmy, M. W.; Haroun, M.; Sabra, S. A. Simultaneous Encapsulation of Dasatinib and Celecoxib into Caseinate Micelles towards Improved in Vivo Anti-Breast Cancer Efficacy with Reduced Drug Toxicity. *J. Drug Delivery Sci. Technol.* **2023**, *87*, No. 104807.

(22) Hefny, S. M.; El-Moselhy, T. F.; El-Din, N.; Ammara, A.; Angeli, A.; Ferraroni, M.; El-Dessouki, A. M.; Shaldam, M. A.; Yahya, G.; Al-Karmalawy, A. A.; Supuran, C. T.; Tawfik, H. O. A New

Framework for Novel Analogues of Pazopanib as Potent and Selective Human Carbonic Anhydrase Inhibitors: Design, Repurposing Rational, Synthesis, Crystallographic, in Vivo and in Vitro Biological Assessments. *Eur. J. Med. Chem.* **2024**, *274*, No. 116527.
(23) Zang, J.; Liang, X.; Huang, Y.; Jia, Y.; Li, X.; Xu, W.; Chou, C. J.; Zhang, Y. Discovery of Novel Pazopanib-Based HDAC and VEGFR Dual Inhibitors Targeting Cancer Epigenetics and Angiogenesis Simultaneously. *J. Med. Chem.* **2018**, *61* (12), 5304−5322.
(24) Venkova, L.; Aliper, A.; Suntsova, M.; Kholodenko, R.; Shepelin, D.; Borisov, N.; Malakhova, G.; Vasilov, R.; Roumiantsev, S.; Zhavoronkov, A.; Buzdin, A. Combinatorial High-Throughput Experimental and Bioinformatic Approach Identifies Molecular Pathways Linked with the Sensitivity to Anticancer Target Drugs. *Oncotarget* **2015**, *6* (29), 27227−27238.
(25) Xue, D.-Q.; Zhang, X.-Y.; Wang, C.-J.; Ma, L.-Y.; Zhu, N.; He, P.; Shao, K.-P.; Chen, P.-J.; Gu, Y.-F.; Zhang, X.-S.; Wang, C.-F.; Ji, C.-H.; Zhang, Q.-R.; Liu, H.-M. Synthesis and Anticancer Activities of Novel 1,2,4-Triazolo[3,4-a]phthalazine Derivatives. *Eur. J. Med. Chem.* **2014**, *85*, 235−244.
(26) Boda, U.; Guguloth, V.; Mood, S.; Guguloth, H. Copper(I)-Catalyzed Regioselective Synthesis of 1,2,3-Triazole−phthalazine-1,4-Dione Hybrids, and Their Anticancer and Molecular Docking Studies. *Russ. J. Org. Chem.* **2023**, *59* (6), 1064−1070.
(27) Wang, L.; Yilmaz, F.; Yildirim, O.; Schölermann, B.; Bag, S.; Greiner, L.; Pahl, A.; Sievers, S.; Scheel, R.; Strohmann, C.; Squire, C.; Foley, D. J.; Ziegler, S.; Grigalunas, M.; Waldmann, H. Discovery of a Novel Pseudo-Natural Product Aurora Kinase Inhibitor Chemotype through Morphological Profiling. *Adv. Sci.* **2024**, *11* (21), 2309202.
(28) Opitz, R.; Maquet, E.; Huisken, J.; Antonica, F.; Trubiroha, A.; Pottier, G.; Janssens, V.; Costagliola, S. Transgenic Zebrafish Illuminate the Dynamics of Thyroid Morphogenesis and Its Relationship to Cardiovascular Development. *Dev. Biol.* **2012**, *372* (2), 203−216.
(29) Sim, K.-M.; Chung, L.-P.; Tan, K.-L.; Tan, Y.-T.; Kee, X.-L.; Teo, K.-C. One-Pot Multicomponent Synthesis of Hydrazinyl thiazoles Bearing anIsatin Moiety in Aqueous Medium. *Lett. Org. Chem.* **2024**, *21* (2), 192−200.
(30) Qu, H.; Wu, Z.; Zhong, G.; Zhang, Y.; Feng, C.; Xu, K. Multicomponent Synthesis of 5-Cyano-pyrazolo[1,5- *a*]Pyrimidines Enabled by Aerobic Manganese Catalysis. *Adv. Synth. Catal.* **2023**, *365* (6), 871−876.
(31) Zeleke, D.; Damena, T. Advance in Green Synthesis of Pharmacological Important Heterocycles Using Multicomponent Reactions and Magnetic Nanocatalysts (MNCs). *Results Chem.* **2024**, *7*, No. 101283.
(32) Yagnasri, P.; Seetharamaiah, N.; Usha Sri, P. Magneto-rheological Performance of Nano Magnetorheological (MR) Fluid Based on NiFe2O4 Nanoparticles. *NanoWorld J.* **2021**, *7* (1), 1−7.
(33) Huang, W.; Jiang, J.; Mandal, T. Ferrite Nanoparticles: Catalysis in Multicomponent Reactions (MCR). *Synth. Commun.* **2021**, *51* (16), 2397−2422.
(34) Bazrafshan, E.; Dahmardeh, Z.; Mohammadi, L.; NadeemZafar, M.; Dargahi, A.; Pirdadeh, F. Synthesis of Magnesium Oxide Nanoparticles and Its Application for Photocatalytic Removal of Furfural from Aqueous Media: Optimization Using Response Surface Methodology. *Arab. J. Chem.* **2023**, *16* (8), No. 104998.
(35) Khan, S. A.; Alam, Md. Z.; Mohasin, Md.; Ahmad, S.; Salma, U.; Parveen, H.; Mukhtar, S.; Al-Anazi, M.; Alotaibi, F. A.; Abdelaziz, M. A. Ultrasound-Assisted Synthesis of Chalcone: A Highly Sensitive and Selective Fluorescent Chemosensor for the Detection of Fe3+ in Aqueous Media. *J. Fluoresc.* **2024**, *34* (2), 723−728.
(36) Sharma, A.; Gudala, S.; Ambati, S. R.; Mahapatra, S. P.; Raza, A.; L. V, Aruna; Payra, S.; Jha, A.; Kumar, A.; Penta, S.; Banerjee, S. On-Water NiFe 2 O 4 Nanoparticle-Catalyzed One-Pot Synthesis of Biofunctionalized Pyrimidine-Thiazole Derivatives: In Silico Binding Affinity and In Vitro Anticancer Activity Studies. *ChemistrySelect* **2018**, 3 (39), 11012−11019.
(37) Payra, S.; Saha, A.; Banerjee, S. Nano-NiFe $_2$ O $_4$ as an Efficient Catalyst for Regio- and Chemoselective Transfer Hydrogenation of Olefins/Alkynes and Dehydrogenation of Alcohols under Pd-/Ru-Free Conditions. *RSC Adv.* **2016**, *6* (57), 52495−52499.
(38) Mosmann, T. Rapid Colorimetric Assay for Cellular Growth and Survival: Application to Proliferation and Cytotoxicity Assays. *J. Immunol. Methods* **1983**, *65* (1−2), 55−63.
(39) Hussein, A. M.; Gomha, S. M.; El-Ghany, N. A. A.; Zaki, M. E. A.; Farag, B.; Al-Hussain, S. A.; Sayed, A. R.; Zaki, Y. H.; Mohamed, N. A. Green Biocatalyst for Ultrasound-Assisted Thiazole Derivatives: Synthesis, Antibacterial Evaluation, and Docking Analysis. *ACS Omega* **2024**, *9* (12), 13666−13679.
(40) Sadgar, A. L.; Deore, T. S.; Hase, D. V.; Jayaram, R. V. Graphene Oxide Pickering Emulsion − A Novel Reaction Medium for the Synthesis of 2-Aminothiazole. *ChemistrySelect* **2021**, *6* (44), 12446−12454.

https://doi.org/10.1021/acsomega.4c05587
ACS Omega 2024, 9, 38262−38271